Magnetotransport, thermoelectric power, thermal conductivity and specific heat of $Pr_{2/3}Sr_{1/3}MnO_3$ manganite

Neeraj Panwar,[1,2] Ashok Rao,[3] R. S. Singh,[4] W. K. Syu,[5] N. Kaurav,[5] Y.-K. Kuo,[5,a),b)] and S. K. Agarwal[1,a),c)]

[1]*Superconductivity and Cryogenics Division, National Physical Laboratory, Dr. K. S. Krishnan Road, New Delhi-110012, India*
[2]*Department of Physics, Indian Institute of Technology, New Delhi-110016, India*
[3]*Department of Physics, Manipal Institute of Technology, Manipal-576104, India*
[4]*Department of Physics, JNV University, Jodhpur-342001, India*
[5]*Department of Physics, National Dong-Hwa University, Hualien 974, Taiwan*

(Received 20 December 2007; accepted 20 August 2008; published online 23 October 2008)

Magnetotransport and thermal studies of $Pr_{2/3}Sr_{1/3}MnO_3$ polycrystalline sintered bulk sample are reported here. The resistivity $\rho(T)$ and thermoelectric power $S(T)$ data show an insulator to metal (I-M) phase transition at $T_P \approx 294$ K and $T_S \approx 290$ K, respectively. Magnetization measurement confirms that the sample undergoes a transition from paramagnetic to ferromagnetic phase at a defined Curie temperature $T_C = 280$ K. A substantial increase in magnetoresistance from 2.5% at 280 K to 5% at 77 K has been noticed in a low magnetic field 0.15 T. Small polaron hopping model is found to be operative above the transition temperature T_P, whereas electron-electron and electron-magnon scattering processes govern the low temperature metallic behavior. A detailed analysis of thermoelectric power in the ferromagnetic regime suggests that the complicated temperature dependence of S may be understood on the basis of electron-magnon scattering. A transition from decreasing high temperature thermal conductivity (due to local anharmonic distortions associated with small polarons), to an increasing thermal conductivity (due to decreasing of phonon-phonon scattering) and thereafter a peak at ~100 K (signifying a crossover from Umklapp to defect-limited scattering) have also been noticed. Specific heat measurements depict a pronounced anomaly near the T_C, indicating the magnetic ordering and magnetic inhomogeneity in the sample. © *2008 American Institute of Physics*. [DOI: 10.1063/1.2992521]

I. INTRODUCTION

Colossal magnetoresistive (CMR) effect in manganite perovskites has attracted considerable attention worldwide due to their peculiar physical properties and potential applications.[1–3] Complete spin polarization due to their half metallic character can be a significant utility factor in the spin based electronic industry.[4] However, the observation of the CMR effect at low temperatures and under the application of high magnetic field (~7T) have hampered their practical utility so far. Efforts are being made to obtain MR effect at low magnetic field values and near room temperature.[5,6] In polycrystalline manganites, occurrence of low field MR due to spin-polarized tunneling[7] or spin dependent scattering[8] of the carriers at the grain boundaries has been reported which makes polycrystalline materials superior candidates over the single crystalline/epitaxial thin film manganite materials. Besides this, various mechanisms working in different temperature regimes need also to be identified to get a clear understanding of such materials from the viewpoint of physics. MR phenomenon in manganite materials has been explained qualitatively by the double-exchange interaction between Mn^{+3}/Mn^{+4} ions via oxygen ion.[9] To explain the insulator-metal (I-M) transition and magnitude of MR, one needs to take into account the electron-phonon coupling due to the fact that Mn^{+3} ion is of Jahn–Teller (JT) type.[10] Recent experimental results including transport measurements,[11] isotope effects,[12] and microscopic techniques[13] have provided strong evidence to the existence of polarons (small or large) in the high temperature paramagnetic insulating region. Conduction of these polarons can be an adiabatic or nonadiabatic process.[14]

Some researchers have also explained the high temperature insulating region by Mott's three-dimensional variable range hopping.[15–17] The metallic region has been explained on the basis of electron-electron and electron-magnon scattering processes.[16] However, merely on the basis of electrical transport measurements it is very difficult to confirm the exact type of mechanisms operating in insulating/metallic regimes. It is known that thermoelectric power (TEP) measurements $S(T)$ are sensitive to the type of charge carriers, while thermal conductivity measurements $\kappa(T)$ would provide valuable information about the various scattering processes of thermal carriers. Specific heat measurements $C_P(T)$, on the other hand, are a direct probe of the occurrence of thermodynamical phase transitions. To investigate all these aspects and study the magnetotransport behavior on the application of low fields, we have carried out a systematic study of electrical, magnetotransport, magnetization, and thermal properties (S, κ, and C_P) on $Pr_{2/3}Sr_{1/3}MnO_3$ (PSMO) manga-

a)Authors to whom correspondence should be addressed.
b)Electronic mail: ykkuo@mail.ndhu.edu.tw. Tel.: 91-11-45608276. FAX.: 91-11-25726938.
c)Electronic mail: prof.agarwal@gmail.com.

nite exhibiting *I-M* transition near room temperature. Therefore thorough investigations of such properties would be rewarding before its utilization in any room temperature device applications such as low field magnetic sensors.

II. EXPERIMENTAL DETAILS

Polycrystalline PSMO material was synthesized through conventional solid-state reaction route with powders of Pr_6O_{11}, $SrCO_3$, and MnO_2 as the starting materials. Stoichiometric mixtures of powders were ground and calcined several times between 900 and 1000 °C for 15 h with intermediate grindings. The pellets of the pressed powder thus obtained were finally sintered at 1260 °C for 20 h and then cooled to room temperature in the furnace. X-ray diffraction (XRD) data were collected at room temperature from 20° to 80° with a 2θ step of 0.05° using a Rigaku diffractometer with Cu $K\alpha$ radiation. To check the surface morphology and the stoichiometric ratio, a scanning electron microscope (SEM) attached with energy dispersive analysis through x rays (EDAXs) LEO SEM 440 system operating at 20 kV was used. Electrical resistivity with and without magnetic field (0.15 T) was recorded using the standard four-probe method from 77 to 350 K with the field applied parallel to the current direction. MR has been calculated through the relation

$$\mathrm{MR}(\%) = \left[\frac{\rho_{(0)} - \rho_{(H)}}{\rho_{(0)}}\right] \times 100, \quad (1)$$

where $\rho_{(H)}$ and $\rho_{(0)}$ are the electrical resistivities with and without magnetic field, respectively. Magnetization measurement was carried out from 10 to 350 K under the application of 0.1 T magnetic field in the zero field cooled configuration in a Quantum Design magnetometer. TEP and thermal conductivity measurements were carried out simultaneously from 8 to 350 K in a closed cycle refrigerator by using a direct-heat pulse technique. Specific heat was measured from 70 to 350 K with a high resolution ac calorimeter, using chopped light as heat source. Details of the thermal measurements techniques are described elsewhere.[18]

III. RESULTS AND DISCUSSION

Figure 1 shows the XRD pattern of PSMO sample including the experimental and Rietveld calculated results.[19] Rietveld refinement has confirmed the phase purity of the material possessing orthorhombic structure with *Pbnm* space group and the lattice parameters are $a = 5.4540(\pm 0.006\%)$ Å, $b = 5.4850(\pm 0.006\%)$ Å, and $c = 7.7080(\pm 0.007\%)$ Å. Scanning electron micrograph of the sample exhibits the granular morphology with an average grain size of ~3 μm (Fig. 2). No impurity is detected by EDAX and it gives the Pr/Sr cationic ratio of 0.67/0.33. Temperature dependence of electrical resistivity $\rho(T)$ of the PSMO sample in zero field is shown in Fig. 3(a). An *I-M* transition (T_P) is observed around 294 K, which is slightly higher than the one reported earlier,[20] depicting better quality of the synthesized material. The MR in the application of low magnetic field of 0.15 T, as calculated using Eq. (1), is also shown in Fig. 3(a). MR curve exhibits a pronounced

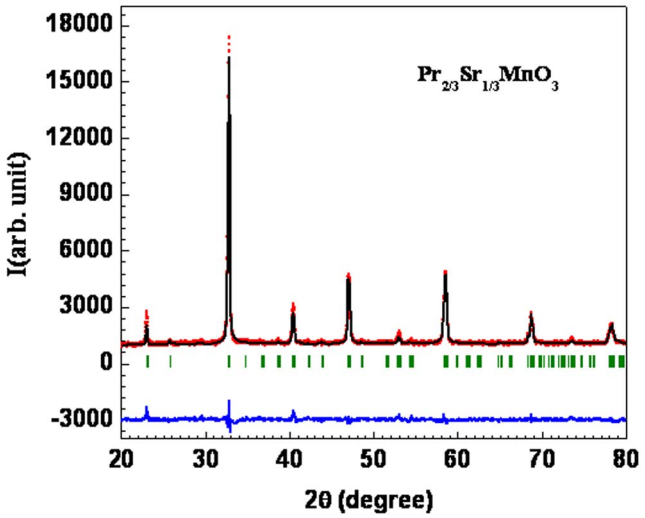

FIG. 1. (Color online) XRD pattern of PSMO system. The observed intensities are shown by dots (red) and the calculated (Rietveld) are shown by the solid line. Blue line at the bottom indicates the difference between the experimental and refined patterns. The vertical bars indicate the expected reflections.

peak near 280 K with a value of about 2.5%, while it is about 5% at 77 K. Below T_P, it increases almost linearly with the decrease in temperature. This is typical feature of the polycrystalline manganite materials and has been attributed to the increased spin polarization with lowering of temperature. MR variation with magnetic field carried out at 77 K also shows the behavior of spin-polarized tunneling as it increases sharply at low magnetic fields and shows a tendency to saturate at higher magnetic fields [inset I, Fig. 3(a)]. Figure 3(b) shows the magnetization variation with temperature for the PSMO sample. The paramagnetic-ferromagnetic (FM) transition temperature (T_C) as obtained from the differentiation [inset Fig. 3(b)] of the magnetization data is 280 K under the magnetic field of 0.1 T. The dip in magnetization below 100 K has been attributed to the ordering of the Pr sublattices.[21]

The variation of TEP $S(T)$ with temperature of PSMO is shown in Fig. 4. Large negative S at high temperatures and

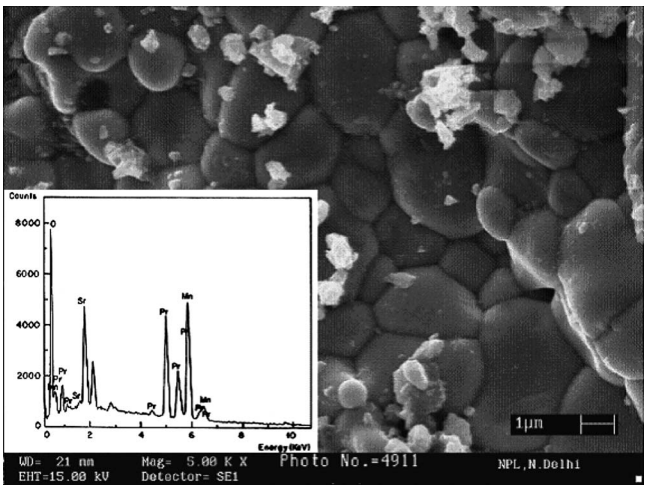

FIG. 2. SEM and EDAX of PSMO.

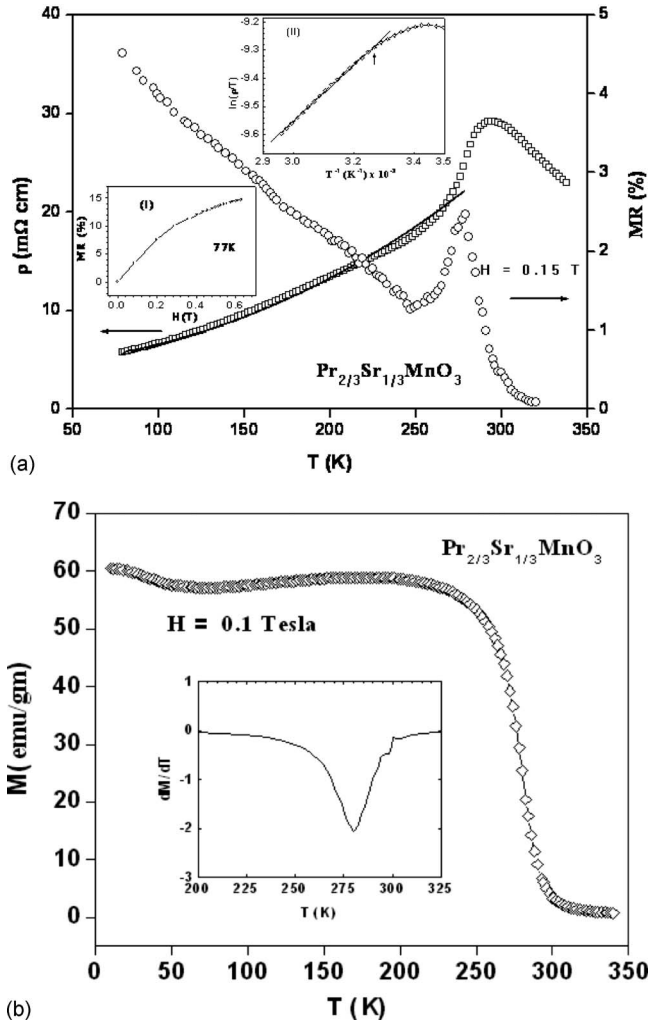

FIG. 3. (a) Electrical resistivity (left) and MR (right) variation with temperature of PSMO. Inset I shows MR variation with magnetic field at 77 K. Inset II shows the electrical resistivity fitting above T_P using Eq. (2). (b) Magnetization variation with temperature of PSMO sample. The inset shows dM/dT vs T curve.

small positive S at low temperatures are reminiscent of the insulating and metallic characters, respectively. With decreasing temperature the magnitude of S decreases sharply around 290 K (T_S), signifying the occurrence of a transition from the high temperature insulating to low temperature metallic state. It is noted that T_S is very close to the electrical resistivity transition temperature T_P. A crossover (indicated by a vertical arrow) from electron-to hole-like conduction is also noticed at 227 K (T^*). With lowering of temperature below T^*, $S(T)$ increases, reaches a broad hump, and then starts to decrease sharply below 30 K. A likely explanation of the origin of broad hump and sharp decrease in TEP at low temperature in PSMO originated from the magnon drag and bare diffusion, respectively, which we will discuss later.

Based on the electrical resistivity and TEP data, we have explored various mechanisms operating in both the insulating and metallic regions. It is worth mentioning that the effect of JT distortion in manganite systems generally results in the possibility of strong electron-phonon coupling and hence the formation of polarons.[10] Therefore, charge carriers in the insulating region, above T_P, are not itinerant and transport properties are governed by thermally activated carriers (polarons).[22] In the framework of the polaron hopping model, E_ρ is the sum of the activation energy required for the creation of carriers and activating the hopping of the carriers and E_S is the energy required to activate the hopping of carriers. The difference in these activation energies, E_ρ and E_S, gives the polaron hopping energy $[W_H=(E_\rho-E_S)]$. For the applicability of the polaron conduction model in the insulating region, we therefore need to check the criteria $E_\rho > E_S$. We have fitted the electrical resistivity data above T_P ($T > \theta_D/2$; θ_D is the Debye temperature equal to twice the temperature, where $\ln(\rho/T^n)$ versus $1/T$ curve deviates from linearity) using the polaron hopping model[22]

$$\rho = \rho_\alpha T^n \exp\left(\frac{E_p}{k_B T}\right), \tag{2}$$

where $\rho_\alpha=[k_B/\nu^{\mathrm{ph}}Ne^2R^2C(1-C)]\exp(2\alpha R)$, k_B is the Boltzmann constant, n is 1 for adiabatic and 1.5 for nonadiabatic processes, N is the number of ion sites per unit volume (obtained from density data), R is the average intersite spacing given by $R=(1/N)^3$, C is the fraction of sites occupied by a polaron, α is the electron wave function decay constant, and ν_{ph} is the optical phonon frequency (estimated from the relation $h\nu_{\mathrm{ph}}=k_B\theta_D$,). Inset II of Fig. 3(a) shows $\ln(\rho/T)$ versus $1/T$ graph for the PSMO system. E_ρ thus obtained is given in Table I. Similarly we have fitted the $S(T)$ data above T_S (shown in inset I of Fig. 4) with Mott's relation[22]

$$S(T) = \frac{k_B}{e}\left[\frac{E_S}{k_B T} + \alpha\right], \tag{3}$$

where the constant α is related to the kinetic energy of the polarons.[23] $\alpha<1$ suggests the conduction due to small polaron hopping (SPH) whereas $\alpha>2$ corresponds to the case of large polaron hopping.[22] The fitting is shown in the inset of Fig. 4 and the deduced parameters E_S and α are listed in Table I. The fitting results ($E_\rho > E_S$ and $\alpha<1$) confirm the

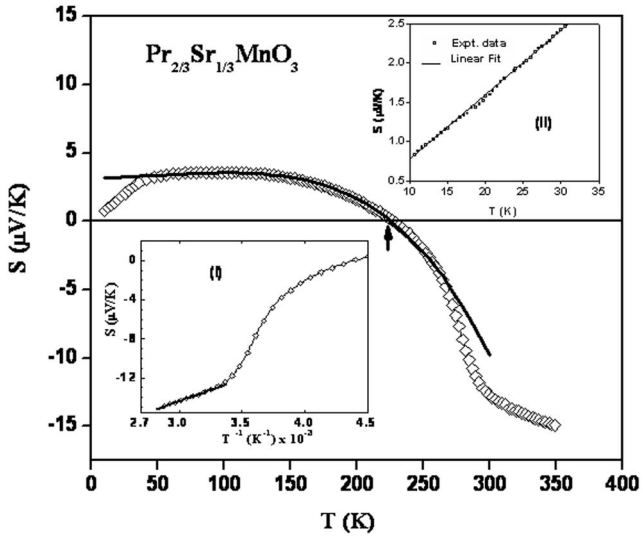

FIG. 4. (Color online) TEP as a function of temperature for PSMO. Inset I shows the fitting above T_S with Eq. (3). In inset II, a linear T dependence of S at low temperatures is seen.

TABLE I. Various fitting parameters obtained after fitting electrical resistivity and TEP data with Eqs. (2)–(5). ± in the brackets represents the fitting errors.

E_ρ (meV)	E_S (meV)	α	ρ_0 (mΩ cm)	ρ_2 (mΩ cm K^{-2}) $\times 10^{-4}$	$\rho_{4.5}$ (mΩ cm K$^{-4.5}$) $\times 10^{-12}$	S_0 (μV K^{-1})	$S_{3/2}$ (μV K$^{-5/2}$) $\times 10^{-4}$	S_4 (μV K^{-5}) $\times 10^{-9}$
85.69	4.59	−0.33	4.40	2.18	8.5	3.17	5.8	−1.97
±0.80	±0.05	±0.02	±0.01	±0.01	±0.2	±0.02	±0.2	±0.01

carrier conduction through the hopping of small polarons in the insulating region.

In the metallic regime (below T_P), the electrical resistivity data [Fig. 3(a)] are found to obey the following relation:

$$\rho = \rho_0 + \rho_2 T^2 + \rho_{4.5} T^{4.5}, \quad (4)$$

where ρ_0 is the residual resistivity arising from the temperature independent processes such as domain wall, grain boundary, vacancies, etc.[24,25] The second term represents the electron-electron scattering[24] whereas the last term stands for the two-magnon scattering process in the FM phase.[26] We have shown the total contribution along with the experimental data in Fig. 3(a). The fitting results, given in Table I, indicate that the metallic region is mainly governed by the electron-electron scattering process as $\rho_2 T^2 = 8.7$ mΩ cm is much larger than $\rho_{4.5} T^{4.5} = 0.19$ mΩ cm calculated at any particular temperature, $T = 200$ K.

Although the contribution from electron-magnon scattering is less as compared to electron-electron scattering, other scattering channels such as spin wave scattering may still be present in the metallic phase. To verify the above argument we have also fitted the measured TEP data in the metallic region using the following relation:[27,28]

$$S(T) = S_0 + S_{3/2} T^{3/2} + S_4 T^4, \quad (5)$$

where S_0 (value of S at $T = 0$ K) is inserted to account for the problem of truncating the low temperature data and $T^{3/2}$ dependence is attributed to electron-magnon scattering process. The origin of the term $S_4 T^4$ may be due to the spin wave fluctuations in the FM phase. In FM state, electrons are scattered by spin waves. Analogous to the phonon drag effects, the electron-magnon interaction produces magnon drag. As the magnon drag effect is approximately proportional to the magnon specific heat, one expects a $T^{3/2}$ contribution in S for the FM system.[27,28] We have fitted our temperature dependent $S(T)$ data to the Eq. (5) and the representative fitting curve is shown in Fig. 4. Our analysis gives reasonable fitting result to experimental data only up to 30 K and it cannot account the sharp fall of experimental data as temperature decreases further. In fact, below 30 K, the TEP is found to follow $S \propto T$ (i.e., bare metallic TEP as shown in inset II of Fig. 4) rather than the Eq. (5). The fitting parameters given in Table I are in good accord with the reported data.[27,28] It is clear that $S_{3/2}$ is nearly five orders of magnitude larger than S_4, implying the second term in Eq. (5) dominates the transport mechanism in FM region below T_C.

It is instructive to mention that the phonon drag effect in these alloys could also play a role in the TEP. We argue that the origin of broad hump in intermediate temperature range presented here originated from the magnon drag (electron-magnon scattering) and not by phonon drag effects. Since at low temperatures, the contribution in S due to the phonon drag should be proportional to the lattice specific heat ($S \propto T^3$), therefore, we attempted to include phonon drag term in the calculations, but such an effort gives no significant improvement to the overall fit. Therefore, based on the analyses of $\rho(T)$ and $S(T)$ data, it can be concluded that transport mechanism in FM phase is most likely dominated by the electron-magnon scattering mechanism.

Hence, based on the above discussion we are able to correlate the transport mechanisms in the low and high temperature regimes for the PSMO manganites, respectively. The high temperature resistivity analysis indicates that the transport mechanism of charge carriers is better described by the SPH model. This is further supported by the TEP analysis in the framework of SPH model in the insulating state. On the other hand, the carrier transport behavior of PSMO has the characteristics of a metal at low temperatures, and the analyses of $\rho(T)$ and $S(T)$ data reveal that in the metallic state, electron-electron and electron-magnon interactions dominate the electrical and thermal transport.

Figure 5 shows the temperature dependent thermal conductivity $\kappa(T)$ of PSMO manganite. The magnitude of $\kappa(T)$, typically of amorphous materials,[29] lies in the range of 16–42 mW/cm K in the temperature range of study, and is consistent with other reported values.[30–32] For a crystalline solid, such low value of thermal conductivity can be thought to originate from random, noncentral distortions of the lattice, resulting in high degree of disorder. In manganites, such

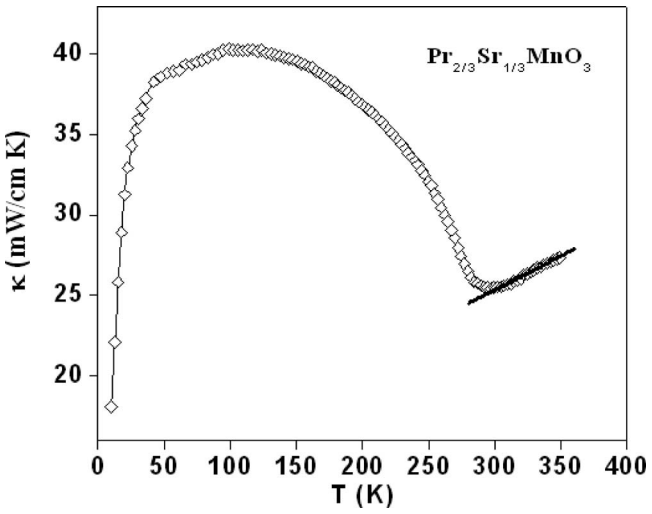

FIG. 5. Thermal conductivity as a function of temperature for PSMO.

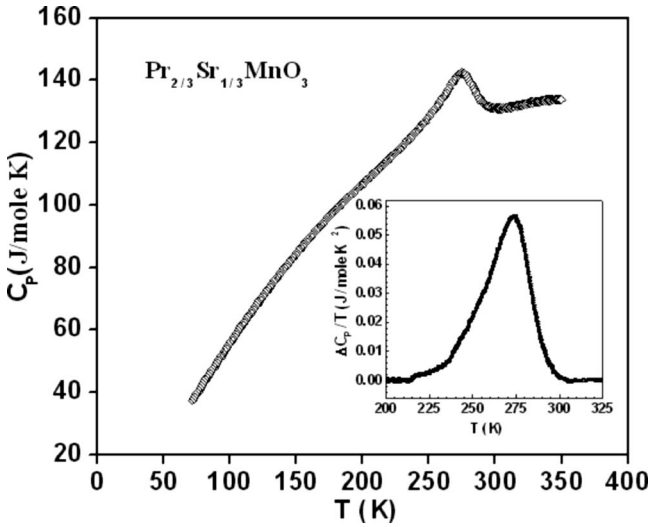

FIG. 6. Specific heat vs temperature for PSMO. The inset shows the specific heat jump with background subtracted.

a scenario may be attributed to the JT distortions of the $Mn^{+3}O_6$ octahedra. $\kappa(T)$ decreases with decreasing temperature down to T_κ (close to T_P and T_S), which is unusual since the high temperature thermal conductivity of the crystalline insulators is mostly a decreasing function of temperature and cannot be attributed to high temperature electron or phonon processes. Such an unusual behavior of $\kappa(T)$ above T_κ may be attributed to the local anharmonic lattice distortions associated with small polarons.[30] Moreover, above T_κ thermal conductivity $\kappa(T)$ can be parametrized by the expression $\kappa=\kappa_0 \exp(T/T')$, where $\kappa_0=15.65$ mW/cm K and $T'=625$ K. In Fig. 5, the solid line represents the fit with this relation in the high temperature region. It is seen that $\kappa(T)$ increases with decreasing temperature below T_κ, presumably due to the reduction in phonon-phonon scattering (Umklapp process) as a result of the JT distortions, which gets delocalized along with the charge carriers. On the other hand, the low temperature peak around 100 K in $\kappa(T)$ can be ascribed to a crossover from Umklapp to defect-limited scattering.[33] In general, the total thermal conductivity for ordinary metals and semimetals is sum of electronic and lattice terms. The electronic thermal conductivity κ_e can be evaluated using the Wiedemann–Franz (WF) law $\kappa_e\rho/T=L$. Here ρ is the dc electrical resistivity and the Lorentz number L is 2.45×10^{-8} W Ω/K^2. Therefore, using the above W-F formula electronic thermal conductivity κ_e at any particular temperature (say 200 K, where the value of electrical resistivity ρ is 13.45 mΩ cm) comes out to be 0.36 mW/cm K, which is just ~1% of the total thermal conductivity κ at that temperature. Hence, the measured κ is suggested to arise from phonons, the contribution of the charge carriers being negligible.

The temperature dependent specific heat $C_P(T)$ of PSMO is illustrated in Fig. 6. The measured data are in accord with the earlier reported results.[32,34] Below T_P, a pronounced peak at 276 K is noticed. The transition temperature, defined as the peak position, being lower than the corresponding *I-M* transition temperature T_P reflects that the specific heat anomaly is related to the magnetic ordering in the sample due to paramagnetic-FM transition [Fig. 3(b)]. The specific heat jump ΔC_{mag} (inset of Fig. 6) and the entropy change ΔS near the transition can be estimated by subtracting a smooth line tangential to both the end points of the peak. Entropy change ΔS calculated by integrating the area under $\Delta C_{\text{mag}}/T$ comes out to be 1.866 J/mole K (or $0.225R$, where R is the ideal gas constant), which is almost one third of the theoretical value of (R ln 2) for the complete alignment of the spins in the FM phase. This discrepancy can be attributed to the magnetic inhomogeneity or partially canted spin state of the material. It has been pointed out that the relative spin wave (magnon) contribution plays a substantial role in the temperature close to T_P (or T_C) where the specific heat anomaly ΔC_{mag} represents a considerable fraction of the total specific heat.[35] Therefore, in the region of thermal conductivity anomaly, it is reasonable to assume that the magnon mean free path is independent of temperature and we could correlate the magnon contribution in the observed thermal conductivity anomaly at T_C with the corresponding specific heat anomaly by the expression $\Delta\kappa_m=(1/3)\Delta C_{\text{mag}}(v_m)^2\tau_m$, where v_m and τ_m are the velocity and lifetime of long wavelength spin wave, respectively. Using the values $\Delta C_{\text{mag}}=15.2$ J/mole K at $T=276$ K, the long wavelength spin wave velocity $v_m=600$ m/s and the long wavelength spin wave lifetime $\tau_m=2\times10^{-12}$ s,[36] $\Delta\kappa_m=0.48\times10^{-2}$ mW/cm K is obtained. The value of $\Delta\kappa_m$ at T_C is negligible compared to the total thermal conductivity. We thus assert that the phonons are the sole carriers of heat transport in thermal conduction for PSMO.

IV. CONCLUSIONS

Systematic magnetotransport and thermal studies have been carried out on the orthorhombic PSMO polycrystalline perovskite manganites. The resistivity $\rho(T)$ and TEP $S(T)$ data show an insulator to metal (*I-M*) phase transition at $T_P\approx294$ K and $T_S\approx290$ K, respectively. Magnetization measurement confirms that the sample undergoes a transition from paramagnetic to FM phase at a defined Curie temperature of $T_C=280$ K. MR at 280 K of ~2.5% value has been noticed in a low magnetic field of 0.15 T, which increases further to ~5% at 77 K. Analyses of electrical resistivity and TEP in different temperature regimes reveal that the conduction of charge carriers in the paramagnetic insulating region (above T_P) is governed by the SPH mechanism. On the other hand, in the metallic region (below T_P), electrical and thermal transport are governed by the electron-electron and electron-magnon scatterings. The anomalous behavior of thermal conductivity at high temperatures has been attributed to the local anharmonic distortions due to the small polarons. Sudden increase in thermal conductivity during the phase transition is attributed to arise from the decrease in phonon-phonon scattering. The broad peak in $\kappa(T)$ at ~100 K corresponds to a crossover from the Umklapp to defect-limited scattering. Specific heat anomaly below T_P is associated with the magnetic ordering and magnetic inhomogeneity in the sample.

ACKNOWLEDGMENTS

The authors are thankful to the Director, National Physical Laboratory, New Delhi, for his support and keen interest in the work. The authors are also thankful to their colleagues Dr. H. Kishan and Dr. V. P. S. Awana for the Rietveld analysis, Dr. R. Kishore for SEM/EDAX, and Dr. A. Banerjee of DAE-CSR, Indore, for magnetization measurements. One of the authors (N.P.) is grateful to the Council of Scientific and Industrial Research, New Delhi, for the grant of a Senior Research Fellowship. Thermal measurements are supported by the National Science Council of Taiwan under Contract No. NSC-96-2112-M-259-004 (Y.K.K.).

[1]R. von Helmolt, J. Wecker, B. Holzapfel, L. Schultz, and K. Samwer, Phys. Rev. Lett. **71**, 2331 (1993).
[2]S. Jin, T. H. Tiefel, M. McCormack, R. A. Fastnacht, R. Ramesh, and L. H. Chen, Science **264**, 413 (1994).
[3]Y. Xu, U. Memmert, and U. Hertmann, Sens. Actuators, A **91**, 26 (2001).
[4]G. Prinz, Phys. Today **48**(4), 58 (1995).
[5]X.-B. Yuan, Y.-H. Liu, C.-J. Wang, and L.-M. Mei, Appl. Phys. Lett. **88**, 042508 (2006).
[6]X.-B. Yuan, Y.-H. Liu, N. Yin, C.-J. Wang, and L.-M. Mei, J. Phys. D **39**, 1028 (2006).
[7]H. Y. Hwang, S.-W. Cheong, N. P. Ong, and B. Batlogg, Phys. Rev. Lett. **77**, 2041 (1996).
[8]A. Gupta, G. Q. Gong, G. Xiao, P. R. Duncombe, P. Lecoeur, P. Trouilloud, Y. Y. Wang, V. P. Dravid, and J. Z. Sun, Phys. Rev. B **54**, R15629 (1996).
[9]C. Zener, Phys. Rev. **82**, 403 (1951).
[10]A. J. Millis, P. B. Littlewood, and B. I. Shraiman, Phys. Rev. Lett. **74**, 5144 (1995).
[11]G. J. Snyder, C. H. Booth, F. Bridges, R. Hiskes, S. DiCarolis, M. R. Beasley, and T. H. Geballe, Phys. Rev. B **55**, 6453 (1997).
[12]M. Jaime, H. T. Hardner, M. B. Salamon, M. Rubinstein, P. Dorsey, and D. Emin, Phys. Rev. Lett. **78**, 951 (1997).
[13]A. Shengelaya, G. M. Zhao, H. Keller, and K. A. Muller, Phys. Rev. Lett. **77**, 5296 (1996).
[14]T. Holstein, Ann. Phys. (N.Y.) **8**, 343 (1959).
[15]G.-H. Zheng, Y.-Q. Ma, X.-B. Zhu, and Y.-P. Sun, Solid State Commun. **142**, 217 (2007).
[16]B. C. Zhao, Y. P. Sun, W. J. Lu, J. Yang, X. B. Zhu, and W. H. Song, Solid State Commun. **139**, 209 (2006).
[17]Y.-H. Huang, C.-S. Liao, Z.-M. Wang, X.-H. Li, C.-H. Yan, J.-R. Sun, and B.-G. Shen, Phys. Rev. B **65**, 184423 (2002).
[18]Y.-K. Kuo, C. S. Lue, F. H. Hsu, H. H. Li, and H. D. Yang, Phys. Rev. B **64**, 125124 (2001).
[19]R. A. Young, *The Rietveld Method* (Oxford University Press, Oxford, 1993).
[20]A. K. Heilman, Y. Y. Xue, B. Lorenz, B. J. Campbell, J. Cmaidalka, R. L. Meng, Y. S. Wang, and C. W. Chu, Phys. Rev. B **65**, 214423 (2002).
[21]N. Rama, V. Sankranarayanan, M. Opel, R. Gross, and M. S. R. Rao, J. Alloys Compd. **443**, 7 (2007).
[22]N. F. Mott and E. A. Davis, *Electronic Processes in Non-Crystalline Materials* (Clarendon, Oxford, 1979).
[23]K. Sega, Y. Kuroda, and H. Sakata, J. Mater. Sci. **33**, 1303 (1998).
[24]P. W. Anderson and H. Hasegawa, Phys. Rev. **100**, 675 (1955).
[25]J. M. De Teresa, M. R. Ibarra, J. Blasco, J. Garcia, C. Marquina, P. A. Algarabel, Z. Arnold, K. Kamenev, C. Ritter, and R. von Helmolt, Phys. Rev. B **54**, 1187 (1996).
[26]K. Kubo and N. Ohata, J. Phys. Soc. Jpn. **33**, 21 (1972).
[27]A. Banerjee, S. Pal, S. Bhattacharya, B. K. Chaudhuri, and H. D. Yang, Phys. Rev. B **64**, 104428 (2001).
[28]P. Mandal, Phys. Rev. B **61**, 14675 (2000).
[29]R. Berman, *Thermal Conduction in Solids* (Clarendon, Oxford, 1976), p. 105.
[30]M. Ikebe, H. Fujishiro, and Y. Konno, J. Phys. Soc. Jpn. **67**, 1083 (1998).
[31]D. W. Visser, A. P. Ramirez, and M. A. Subramanian, Phys. Rev. Lett. **78**, 3947 (1997).
[32]L. M. Wang, J.-H. Lai, J.-I. Wu, Y.-K. Kuo, and C. L. Chang, J. Appl. Phys. **102**, 023915 (2007).
[33]P. G. Klemens, in *Solid State Physics*, edited by F. Seitz and D. Turnbull, (Academic, New York, 1958), p. 7.
[34]M. N. Khlopkin, G. K. Panova, A. A. Shikov, V. F. Sinyavskii, and D. A. Shulyatev, Phys. Solid State **42**, 114 (2000).
[35]J. Tanaka and T. Mitsuhashi, J. Phys. Soc. Jpn. **53**, 24 (1984).
[36]J. L. Cohn, J. J. Neumeier, C. P. Popoviciu, K. J. McClellan, and T. Leventouri, Phys. Rev. B **56**, R8495 (1997).